

Review of superior mechanical and corrosion properties of wrought magnesium based materials containing nanoparticles

M. Paramsothy¹, Q. B. Nguyen¹, K. S. Tun¹, R. Balasubramaniam², J. Chan³, R. Kwok³,
J. V. M. Kuma⁴, M. Gupta^{1*}

¹Department of Mechanical Engineering, National University of Singapore, 9 Engineering Drive 1, Singapore 117576

²Department of Materials and Metallurgical Engineering, Indian Institute of Technology,
Kalyanpur, Kanpur 208016, India

³Singapore Technologies Kinetics Ltd (ST Kinetics), 249 Jalan Boon Lay, Singapore 619523

⁴Minerals, Metals & Materials Technology Centre, National University of Singapore, 9 Engineering Drive 1,
Singapore 117576

Received 23 September 2010, received in revised form 29 October 2010, accepted 9 November 2010

Abstract

Magnesium is actively used as a lightweight structural metal in the transport industry. Its use ensures lower fuel consumption, reduced CO₂ emissions and thus a greener earth. This paper describes the multiple beneficial effects of nanoparticle addition to wrought magnesium based systems. Regarding mechanical properties, the effects are either: (a) enhanced ductility or (b) simultaneously enhanced strength and ductility of magnesium. Regarding material degradation, the beneficial effects include: (a) higher dry oxidation resistance and (b) higher salt water corrosion resistance. The results obtained so far clearly indicate the capability of nanoparticles to enhance the properties of wrought magnesium and its alloys in a way never seen before with micron length scale reinforcements.

Key words: magnesium alloys, nanoparticles, mechanical properties, corrosion properties

1. Introduction

Magnesium and aluminium are commonly used light metals in weight-critical structural applications (for example, automotive and aerospace). Mg is about 35 % lighter than Al and both have similar melting points and strengths. Mg has the disadvantage of limited ductility attributed to its HCP structure, while Al is more ductile given its FCC structure. Also, Mg has a lower elastic modulus (40–45 GPa) than Al (69.6 GPa) [1]. Traditional alloying can be used to increase strength and ductility of Mg [2]. Additionally, based on the use of discontinuous reinforcement, many properties of Mg have been improved beyond the limits of alloying [3]. In recent years, three methods that have been tried to improve the strength, ductility and modulus of Mg are in use of: (a) various oxide nanoparticles as well as carbon nanotubes for improving strength and ductility [4–6], (b) Ti and Mo metallic microparticles for improving ductility [7–9] and (c)

SiC ceramic microparticles for improving strength and modulus [10, 11]. Among these three methods, nanoparticle addition has proven to be the most promising in improving the overall mechanical properties of Mg. Regarding degradation, Mg alloys are known to be more prone to: (a) dry oxidation and (b) wet corrosion compared to Al alloys. This can be attributed (respectively) to the relatively: (a) non-adherent oxide film formation and (b) higher electrochemical activity of Mg compared to Al. The addition of Y₂O₃ microparticles may slightly improve the dry oxidation resistance of Mg alloy [12]. However, the effects of other microparticles on the dry oxidation resistance of Mg alloy are not known. It has been shown that the addition of microparticle reinforcement to Mg alloy decreases the wet corrosion resistance of Mg alloy [13–17]. This can be attributed to the relatively cathodic nature of the microparticle reinforcement and related consequent galvanic corrosion of the Mg alloy matrix [13–17]. This further necessitates the need to employ

*Corresponding author: tel.: +65 6516 6358; fax: +65 6779 1459, e-mail address: mpegm@nus.edu.sg

coating technology to sufficiently protect the Mg alloy [18–20]. At present, the effects of nanoparticle addition on the dry oxidation and wet corrosion characteristics of Mg alloys are being studied.

Accordingly, the primary aim of this paper is to describe the multiple beneficial effects of nanoparticle addition to wrought magnesium. Regarding mechanical properties, the effects are either: (a) enhanced ductility or (b) simultaneously enhanced strength and ductility of wrought magnesium. Regarding material degradation, the beneficial effects include: (a) higher dry oxidation resistance and (b) higher salt water corrosion resistance.

2. Experimental

2.1. Materials and processing

In this study, the matrix materials used were: (1) Mg turnings (99.9 + %, supplied by ACROS Organics, New Jersey, USA), (2) AZ31 pieces (nominally 2.40–3.60 wt.% Al, 0.50–1.50 wt.% Zn, 0.15–1.00 wt.% Mn, 0.10 wt.% Si max, 0.10 wt.% Cu max, 0.03 wt.% Ni max, 0.30 wt.% others max, balance Mg, supplied by Alfa Aesar, Massachusetts, USA), (3) AZ31B pieces (nominally 2.94 wt.% Al, 0.87 wt.% Zn, 0.57 wt.% Mn, 0.0112 wt.% Si, 0.0008 wt.% Cu, 0.0005 wt.% Ni, 0.0027 wt.% Fe, balance Mg, supplied by Tokyo Magnesium Co. Ltd., Yokohama, Japan) and (4) ZK60A pieces (nominally 4.80–6.20 wt.% Zn, 0.45 wt.% Zr min, 0.30 wt.% others max, balance Mg, supplied by Tokyo Magnesium Co. Ltd., Yokohama, Japan). The reinforcement materials used were: (1) Al₂O₃ nanoparticles (50 nm size, supplied by Baikowski, Japan), (2) CNT powder (vapour grown, 40–70 nm outer diameter, 94.7 % purity, supplied by Nanostructured & Amorphous Materials Inc, Texas, USA) and (3) Y₂O₃ nanoparticles (29 nm average size, supplied by Nanostructured & Amorphous Materials Inc., Texas, USA). Monolithic Mg, AZ31 and ZK60A (turnings and pieces) as well as related nanocomposites were cast using the DMD method [21]. Ingots of 40 mm diameter were obtained and sectioned into billets. This was followed by hot extrusion at 250 °C or 350 °C into 7 mm or 8 mm rod for further characterization.

2.2. Microstructural characterization

XRD studies were conducted using Cu K α radiation ($\lambda = 1.5406 \text{ \AA}$) with a scan speed of 2°/min in an automated Shimadzu LAB-X XRD-6000 diffractometer to determine the dominant textures in the transverse and longitudinal (extrusion) directions, for selected nanocomposites and relevant monolithic material.

2.3. Tensile testing

Smooth bar tensile properties were determined based on ASTM E8M-05, where axial extensometer was used and crosshead speed was set at 0.254 mm min⁻¹. For each composite system including corresponding monolithic material, round tension test samples of 5 mm diameter and 25 mm gauge length were tested using an MTS 810 machine or Instron 8516 machine. Fractography was performed on the tensile-fracture surfaces using scanning electron microscopy (JEOL JSM-5800 LV SEM and Hitachi S4300 Field Emission SEM).

2.4. Dry oxidation testing

Dry oxidation characteristics of selected nanocomposites and relevant monolithic material were determined using thermogravimetry. Samples having 1 mm \times 3 mm \times 3 mm dimensions were cut from the extruded rods. The samples were initially mechanically ground on 2000-grit silicon carbide impregnated emery paper, washed ultrasonically in acetone, and then dried in ambient air (25 °C). The DTA-TG apparatus (Shimadzu DTG-60H), with an accuracy of 1 μ g, was used to investigate the oxidation behaviour. The specimens were inserted into the DTA-TG machine at room temperature and heated at a ramping rate of 50 °C min⁻¹. The kinetics of weight change was calculated and compared in the laboratory air environment under isothermal conditions in the temperature range of 300–470 °C and for time intervals up to 7 h. The samples that were oxidized were then characterized with the purpose of investigating the morphological characteristics of the oxide layer and interfacial integrity between the matrix and the oxide layer. To provide a meaningful insight into the oxidation behaviour of the monolithic material and its nanocomposites, the test samples were mounted in resin, ground, polished and etched with the purpose of revealing the oxide layer and the grain boundaries for purpose of microstructural examination [22]. A light optical microscope and a scanning electron microscope (Model: FESEM-S4300) equipped with EDS were used to characterize the microstructure.

2.5. Salt water corrosion testing

Salt water corrosion characteristics of selected nanocomposites and relevant monolithic material were determined using potentiostatic electrochemical testing (PET) and electrochemical impedance spectroscopy (EIS). Cylindrical discs were cut from the extruded rods and embedded in epoxy after soldering a copper wire on the sample. Experiments were performed in freely aerated 3.5 wt.% NaCl solution at ambient temperature (25 °C). All experiments were

Table 1. Results of tensile testing of magnesium nanocomposites

Material	0.2 % YS (MPa)	UTS (MPa)	Failure strain/ductility (%)	WOF (MJ m ⁻³) ^a	Reference
<i>Significant enhancement of ductility compared to monolithic material:</i>					
Mg	126 ± 7	192 ± 5	8.0 ± 1.6	–	[49]
Mg/0.23vol.%CNT	128 ± 6	194 ± 9	12.7 ± 2.0	–	[49]
Mg/1.01vol.%CNT	140 ± 2	210 ± 4	13.5 ± 2.7	–	[49]
Mg/1.24vol.%CNT	121 ± 5	200 ± 3	12.2 ± 1.7	–	[49]
AZ31B	201 ± 7	270 ± 6	5.6 ± 1.4	15 ± 3	[22]
AZ31B/0.66vol.%Al ₂ O ₃ (NI) ^b	149 ± 7	215 ± 15	14.6 ± 1.1	31 ± 4	[22]
AZ31B/1.11vol.%Al ₂ O ₃ (NI) ^b	148 ± 11	214 ± 16	25.5 ± 2.2	52 ± 2	[22]
AZ31B/1.50vol.%Al ₂ O ₃ (NI) ^b	144 ± 9	214 ± 16	29.5 ± 1.9	60 ± 3	[22, 36]
ZK60A ^c	139 ± 4	246 ± 4	20.2 ± 2.0	46 ± 4	[38]
ZK60A/1.50vol.%Al ₂ O ₃ ^c	147 ± 8	252 ± 5	25.5 ± 1.0	61 ± 2	[38]
<i>Simultaneous significant enhancement of strength and ductility compared to monolithic material:</i>					
Mg	97 ± 2	173 ± 1	7.4 ± 0.2	11.1 ± 0.3	[30]
Mg/0.22vol.%Y ₂ O ₃	218 ± 2	277 ± 5	12.7 ± 1.3	29.6 ± 3.5	[30]
Mg	97 ± 2	173 ± 1	7.4 ± 0.2	11.1 ± 0.3	[31, 50]
Mg/0.66vol.%Al ₂ O ₃	170 ± 4	229 ± 2	12.4 ± 2.1	30.0 ± 3.2	[31, 50]
Mg/1.11vol.%Al ₂ O ₃	175 ± 3	246 ± 3	14.0 ± 2.4	31.7 ± 6.3	[31, 50]
AZ31	172 ± 15	263 ± 12	10.4 ± 3.9	26 ± 9	[32, 36]
AZ31/1.50vol.%Al ₂ O ₃ (I) ^d	204 ± 8	317 ± 5	22.2 ± 2.4	68 ± 7	[32, 36]
AZ31	172 ± 15	263 ± 12	10.4 ± 3.9	26 ± 9	[35]
AZ31/1.00vol.%CNT	190 ± 13	307 ± 10	17.5 ± 2.6	50 ± 8	[35]

^a Obtained from engineering stress-strain diagram using EXCEL software

^b (NI) refers to non-isolated nature of reinforcement from matrix prior to melting

^c Heat treated at 150°C for 1 h

^d (I) refers to isolated nature of reinforcement from matrix prior to melting

performed in a round bottom cell using a potentiostat PARSTAT 2263 (Princeton Applied Research, IL, USA). The reference electrode used was saturated calomel electrode (SCE, + 241 mV versus standard hydrogen electrode). Two graphite rods were used as counter electrodes. The free corrosion potential of the samples was stabilized before commencement of experiments. In PET, experiments were conducted between ± 250 mV from the free corrosion potential using a scan rate of 0.166 mV s⁻¹. The corrosion rates were determined by the Tafel extrapolation method. In EIS, measurement was performed by applying a sinusoidal potential perturbation of 10 mV at open circuit potential in the frequency range of 100 kHz – 10 mHz.

3. Results and discussion

3.1. Tensile behaviour

Results of mechanical testing are listed in Table 1. Depending on the matrix-reinforcement combination and processing route used, either: (a) ductility or (b) strength and ductility simultaneously were sig-

nificantly enhanced compared to monolithic material. All cases of strength increase can be attributed to well known factors (pertaining to reinforcement) such as: (a) dislocation generation due to elastic modulus mismatch and coefficient of thermal expansion mismatch between the matrix and reinforcement [5, 6, 23, 24, 26, 27], (b) Orowan strengthening mechanism (inclusive of reduction in diameter of intermetallic particles) [23–27] and (c) load transfer from matrix to reinforcement [5, 23, 26, 27]. In the case of AZ31/1.50vol.%Al₂O₃ (I), the enhancement of tensile strength can be first attributed to crystallographic texture difference between the nanocomposite matrix and monolithic material. In comparison of crystallographic texture, monolithic AZ31 exhibited (0 0 0 2) dominant texture in the longitudinal direction unlike AZ31/1.50vol.%Al₂O₃ (I) as listed in Table 2 and shown in Fig. 1. For this (0 0 0 2) basal plane texture, basal slip is made most difficult due to the high critical resolved shear stress (CRSS) for slip based on the 0° angle between the (0 0 0 2) basal plane and the vertical axis [25, 28]. However, non-basal slip was activated during deformation at room temperature due to basal plane alignment along the vertical (force) axis [29]. In the case of AZ31/1.00vol.%CNT, the enhancement of

Table 2. Texture results of AZ31, ZK60A and selected derived nanocomposites based on X-ray diffraction

Material	Section ^a	Plane	Average I/I_{\max} ^b	Reference
AZ31	T	1 0 -1 0 prism	1.00	[32, 35]
		0 0 0 2 basal	0.16	
		1 0 -1 1 pyramidal	0.81	
	L	1 0 -1 0 prism	0.27	
		0 0 0 2 basal	0.93	
		1 0 -1 1 pyramidal	1.00	
AZ31/1.50vol.%Al ₂ O ₃ (I) ^c	T	1 0 -1 0 prism	1.00	[32]
		0 0 0 2 basal	0.18	
		1 0 -1 1 pyramidal	0.72	
	L	1 0 -1 0 prism	0.23	
		0 0 0 2 basal	0.64	
		1 0 -1 1 pyramidal	1.00	
AZ31B/1.50vol.%Al ₂ O ₃ (NI) ^d	T	1 0 -1 0 prism	1.00	-
		0 0 0 2 basal	0.05	
		1 0 -1 1 pyramidal	0.63	
	L	1 0 -1 0 prism	0.27	
		0 0 0 2 basal	1.00	
		1 0 -1 1 pyramidal	0.93	
AZ31/1.00vol.%CNT	T	1 0 -1 0 prism	0.51	[35]
		0 0 0 2 basal	0.17	
		1 0 -1 1 pyramidal	1.00	
	L	1 0 -1 0 prism	0.29	
		0 0 0 2 basal	0.64	
		1 0 -1 1 pyramidal	1.00	
ZK60A ^e	T	1 0 -1 0 prism	0.07	[35]
		0 0 0 2 basal	0.26	
		1 0 -1 1 pyramidal	1.00	
	L	1 0 -1 0 prism	0.21	
		0 0 0 2 basal	0.48	
		1 0 -1 1 pyramidal	1.00	
ZK60A/1.50vol.%Al ₂ O ₃ ^e	T	1 0 -1 0 prism	0.24	[38]
		0 0 0 2 basal	0.14	
		1 0 -1 1 pyramidal	1.00	
	L	1 0 -1 0 prism	0.23	
		0 0 0 2 basal	0.53	
		1 0 -1 1 pyramidal	1.00	

^a T: transverse, L: longitudinal

^b I_{\max} is XRD maximum intensity from either prism, basal, or pyramidal planes

^c (I) refers to isolated nature of reinforcement from matrix prior to melting

^d (NI) refers to non-isolated nature of reinforcement from matrix prior to melting

^e Heat treated at 150°C for 1 h

tensile strength occurred despite the crystallographic texture difference between the nanocomposite matrix and monolithic material. In comparison of crystallographic texture, AZ31/1.00vol.%CNT exhibited (1 0 -1 1) dominant texture in the transverse and longitudinal directions (or (0 0 0 2) basal plane at about

45° angle to vertical axis) unlike monolithic AZ31. For this (1 0 -1 1) pyramidal plane texture, basal slip is made least difficult due to the low CRSS for slip based on the 45° angle between the (0 0 0 2) basal plane and the vertical axis [25, 28].

Considering Mg nanocomposites, the wide range

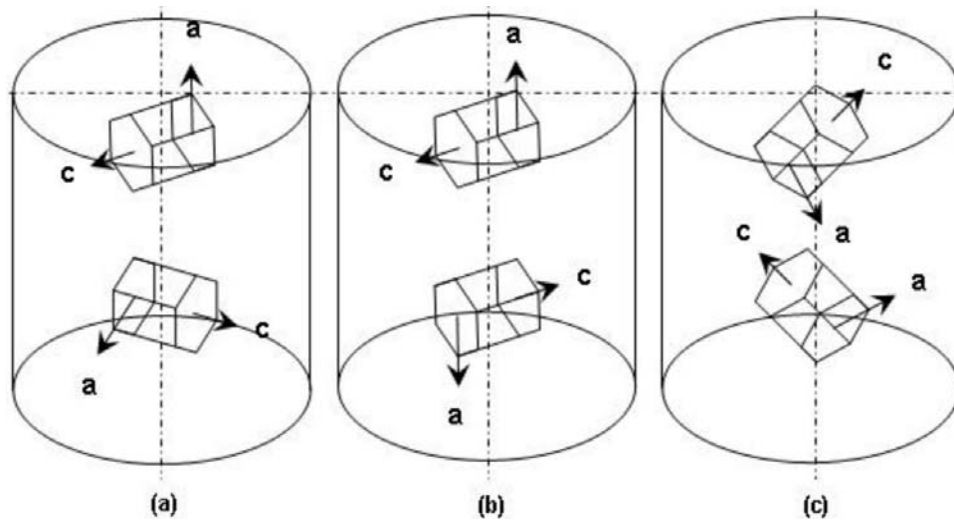


Fig. 1. Schematic diagram showing textures of: (a) monolithic AZ31, AZ31/1.50vol.%Al₂O₃ (I), AZ31B/1.50vol.%Al₂O₃ (NI), (b) monolithic AZ31, AZ31B/1.50vol.%Al₂O₃ (NI) and (c) AZ31/1.00vol.%CNT, monolithic ZK60A, ZK60A/1.50vol.%Al₂O₃ based on X-ray diffraction. In each case, vertical axis is parallel to extrusion direction. Each cell is made up of 2 HCP units having 1 common (0 0 2) basal plane.

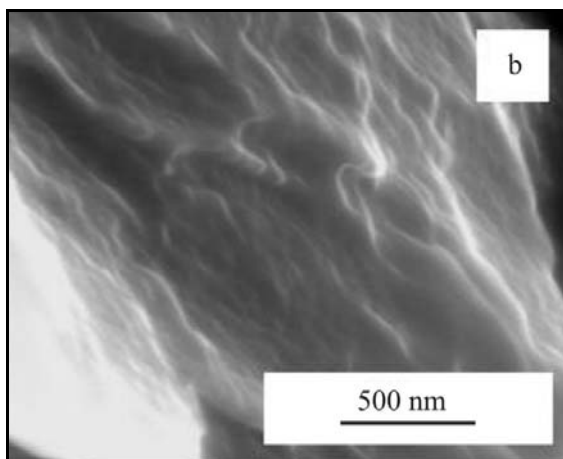
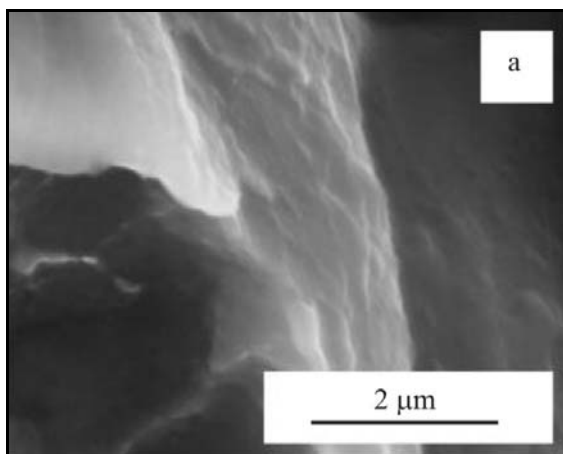


Fig. 2. Representative fractographs of: (a) pure AZ31B and (b) AZ31B/1.50vol.%Al₂O₃ (NI) showing non-parallel or wavy lines indicating non-basal slip.

of failure strain displayed can be attributed to the presence and reasonably uniform distribution of nanoparticles [30, 31]. It has been shown in previous studies that the nanoparticles provide sites where cleavage cracks are opened ahead of the advancing crack front. This: (1) dissipates the stress concentration which would otherwise exist at the crack front and (2) alters the local effective stress state from plane strain to plane stress in the neighbourhood of crack tip [30, 31]. Considering AZ31 nanocomposites, the extreme range of ductility displayed can be similarly attributed to crystallographic texture difference among the nanocomposites. In comparison of crystallographic texture, AZ31/1.50vol.%Al₂O₃ (NI) exhibited (0 0 2) dominant texture in the longitudinal direction unlike AZ31/1.00vol.%CNT. For this (0 0 2) basal plane texture, basal slip is made most difficult due to the high CRSS for slip based on the 0° angle between the (0 0 2) basal plane and the vertical axis. However, non-basal slip was activated during deformation at room temperature due to basal plane alignment along the vertical (force) axis [29, 32]. Here, more slip systems (non-basal ones) become available during deformation in addition to the existing basal slip systems, based on basal plane alignment along the direction of applied force [29, 32–34]. Figure 2 supports this observation of non-basal slip activation up to fracture [22]. Another reason for the significant increase in ductility was the lower size of more rounded intermetallic particles in the nanocomposites compared to pure AZ31 [22, 35, 36]. Roundness is a measure of the sharpness of a particle's edges and corners. The rounder the particle, the lower the extent of stress localization around the particle in the matrix. Breakdown of the intermetallic particles

Table 3. Oxidation rate (mmpy) of monolithic AZ31B and nanocomposite samples calculated following Wagner's model [41] at different temperatures [42]

Materials	Temperature	300 °C	350 °C	400 °C	450 °C	470 °C
AZ31B		1.32	1.89	2.27	4.20	10.03
AZ31B/0.66vol.%Al ₂ O ₃ (NI)		0.65	1.10	1.71	3.51	9.54
AZ31B/1.11vol.%Al ₂ O ₃ (NI)		0.35	0.70	1.28	2.98	7.82
AZ31B/1.50vol.%Al ₂ O ₃ (NI)		0.26	0.46	1.01	2.77	7.58

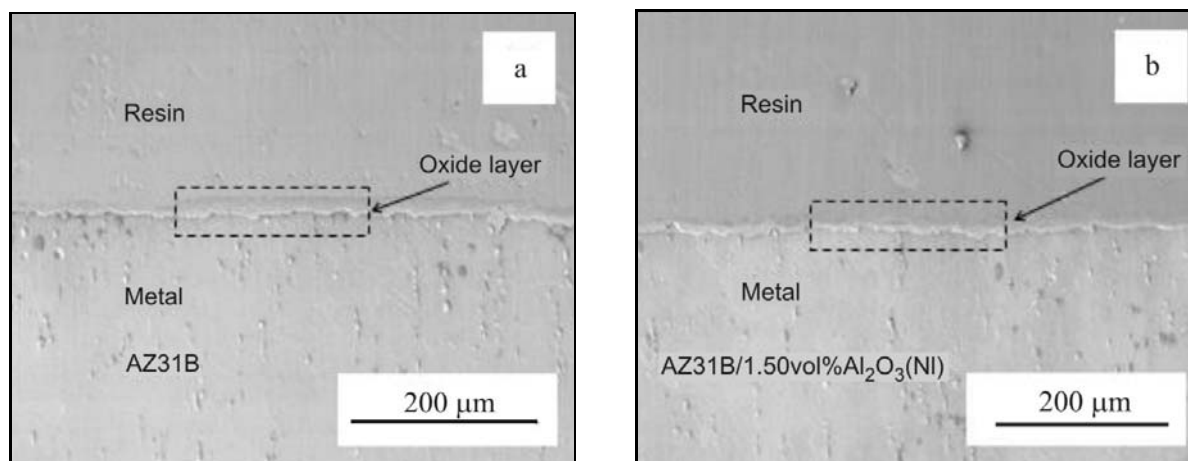


Fig. 3. Cross-sectional images showing MgO oxide layer after 7 h exposure in air at 450 °C in the cases of: (a) monolithic AZ31B and (b) AZ31B/1.50vol.%Al₂O₃ (NI) nanocomposite [42].

located at grain boundaries and the change in their distribution from a predominantly aggregated type to dispersed type can assist in improving ductility [32, 37]. The more the intermetallic particles are dispersed, the lower the presence of voids between the particles (aggregates are generally void-filled in comparison). In the case of AZ31/1.00vol.%CNT, the (0002) basal plane was tilted 45° from the force axis and this enabled basal slip activation very easily during tensile deformation. The case in terms of texture for ZK60A/1.50vol.%Al₂O₃ was similar. However, ductility increase in this nanocomposite can also be attributed to overall ZK60A-Al₂O₃ matrix-particle interfacial relaxation [38]. It has been shown in previous studies that reducing the stress built up at the matrix-particle interface leads to enhanced ductility [39, 40].

3.2. Dry oxidation characteristics

The oxidation rate was calculated using the expression initially put forth by Wagner [41]:

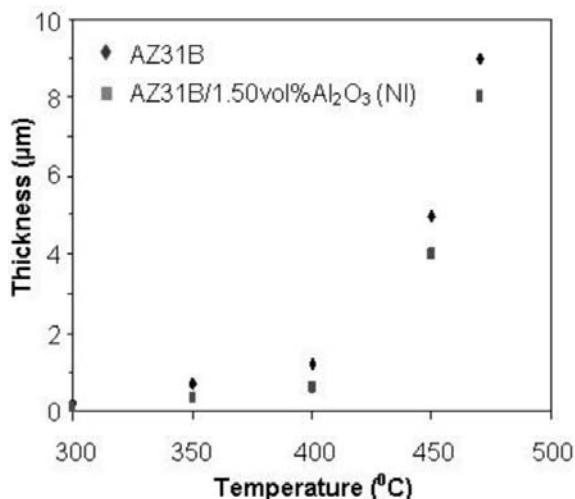
$$\text{mmpy} = 87.6W/DAT, \quad (1)$$

where mmpy is the oxidation rate in mm per year, W is weight loss in mg, D is density of specimen in g cm^{-3} ,

A is area of specimen in cm^2 and T is the exposure time in h. Oxidation rates of monolithic AZ31B and its nanocomposites were calculated using Eq. (1) and summarized in Table 3. The results revealed that the oxidation rate of monolithic AZ31B was significantly reduced with a progressive increase in Al₂O₃ nanoparticle content. The results also revealed that the oxidation rate of the nanocomposite containing 1.5 vol.% Al₂O₃ was well within the acceptable range up to a temperature of 400 °C [41]. The observed reduction in the oxidation rate of alloy AZ31B as a result of the presence of Al₂O₃ nanoparticles can be attributed to the mutually interactive influences of the following: (a) fairly uniform distribution of the Al₂O₃ nanoparticle in the magnesium alloy [22, 43], (b) good interfacial integrity between the reinforcing Al₂O₃ nanoparticle and the magnesium alloy AZ31B metal matrix in terms of debonded region [22, 43], (c) redistribution of smaller second-phase particles (Mg₁₇Al₁₂) within the AZ31B metal matrix [44] and (d) increase in the amount of aluminium in the magnesium solution [44, 45]. A fairly uniform distribution of Al₂O₃ nanoparticles in AZ31B matrix can assist in minimizing the migration of ions to the metal/oxygen interface and thus reducing the oxidation rate. The results of earlier investigations [22, 42] have shown that the addition of Al₂O₃ nanoparticles led to an observ-

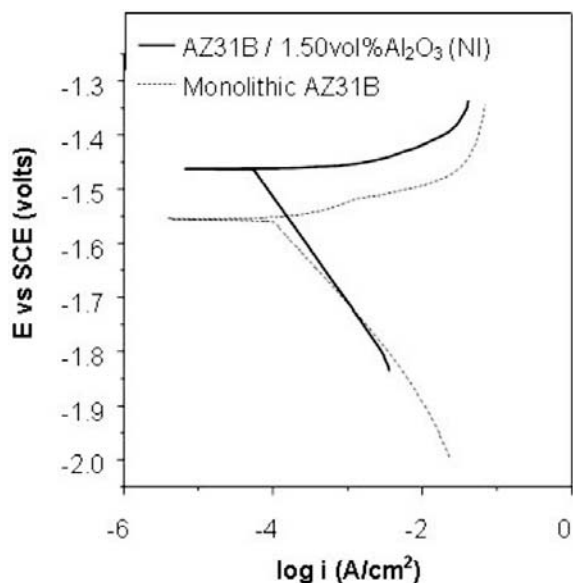
Table 4. Results from polarization plots using Tafel extrapolation method for AZ31B and AZ31B/1.50vol.%Al₂O₃ (NI) nanocomposite in NaCl solution

Materials	ZCP (V vs SCE)	β_a (mV/decade)	β_c (mV/decade)	i_{corr} ($\mu\text{A cm}^{-2}$)	Corrosion rate (mmpy)
AZ31B	-1.52 ± 0.03	26 ± 10	205 ± 27	157 ± 68	27 ± 12
AZ31B/ 1.50vol.%Al ₂ O ₃ (NI)	-1.46 ± 0.00	8 ± 3	191 ± 3	47 ± 8	9 ± 2

Fig. 4. Oxide thickness of monolithic AZ31B and AZ31B/1.50vol.%Al₂O₃ (NI) nanocomposite after exposure for 7 h at different temperatures in ambient atmosphere [42].

able reduction in the volume fraction coupled with a redistribution of the second phase in the metal matrix. This suggests the presence of more aluminium in solid solution resulting in a progressive increase in the oxidation resistance of magnesium alloy AZ31B [44, 45].

A cross-section of the AZ31B and AZ31B/1.50 vol.%Al₂O₃ (NI) nanocomposite after exposure at 450 °C is shown in Fig. 3. The presence of an oxide film on both monolithic AZ31B and its nanocomposite can be readily noticed. In both cases, the film shows good integrity with the base metal and the thickness of the film was marginally lower for the case of the nanocomposite sample. The results shown in Fig. 4 clearly indicate the variation in thickness of the oxide layer for both AZ31B and AZ31B/1.50vol.%Al₂O₃ (NI) nanocomposite. At all temperatures, the thickness of the oxide layer was lower for the composite samples. However, at temperatures over 400 °C, the thickness of the oxide layer for both monolithic and the composite samples increased rapidly suggesting a transition from the protective oxide to a non-protective oxide. The test results clearly indicate that the presence of Al₂O₃ nanoparticles in magnesium alloy AZ31B retards the oxidation rate at all temperatures investigated in this study but could not prevent the transition of the ox-

Fig. 5. Typical Tafel plots for monolithic AZ31B and AZ31B/1.50vol.%Al₂O₃ (NI) nanocomposite in 3.5 wt.% NaCl solution [48].

ide from protective to non-protective at temperatures above 400 °C.

3.3. Salt water corrosion characteristics

Typical polarisation plots are presented in Fig. 5 for monolithic and nanocomposite materials. Parameters derived from the Tafel extrapolation experiments, namely: (a) zero current potential (ZCP), (b) corrosion current density (i_{corr}), (c) anodic and cathodic Tafel slopes β_a and β_c , and (d) corrosion rate (in mm/year) are shown in Table 4. The cathodic Tafel slopes were in the range of 180–230 mV/decade while the anodic Tafel slopes were in the range of 5–35 mV/decade. This indicated that the polarisation behaviour was significantly influenced by the nature of the Mg alloy matrix phase. The low values of anodic slopes indicated extensive pitting tendency in the given medium [46]. The cathodic slopes were used to determine the corrosion rate by extrapolating them to meet the horizontal drawn at the zero current potential. The corrosion current density i_{corr} was lower in the case of nanocomposite material. The corrosion rate of the nano-

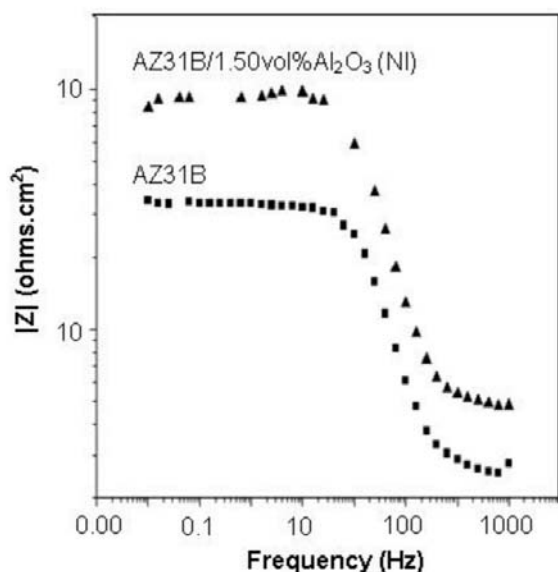


Fig. 6. Bode magnitude plots for monolithic AZ31B and AZ31B/1.50vol.%Al₂O₃ (NI) nanocomposite in 3.5 wt.% NaCl solution [48].

composite was a third that of the monolithic alloy.

The Tafel extrapolation method may not be appropriate for estimating the corrosion rate of Mg and its alloys because of the negative difference effect [47]. Here, deviation of anodic oxidation of Mg alloy away from linear behaviour towards higher anodic current values plays a significant role [47]. Also, hydrogen gas evolution on the Mg alloy surface via: (a) electrochemical means and/or (b) MgH₂ decomposition is believed to play a significant role in this effect [47]. Electrochemical impedance spectroscopy (EIS) was used to independently confirm the superior corrosion resistance of the composite material. The Bode magnitude plots for AZ31B and AZ31B/1.50vol.%Al₂O₃ (NI) nanocomposite in 3.5 wt.% NaCl solution are shown in Fig. 6. The higher polarization resistance of the nanocomposite material is very evident. The polarization resistance is almost twice in the case of the nanocomposite and this confirms its improved corrosion resistance compared to the monolithic alloy. The improved corrosion resistance of the nanocomposite can be attributed to the lower fraction of deleterious Mg₁₇Al₁₂ intermetallic phase in the microstructure of the nanocomposite [48].

4. Conclusions

1. The addition of nanoparticles to magnesium is capable of simultaneously and significantly increasing strength and ductility of magnesium. This is significantly more beneficial compared to microparticle ad-

dition where typically either strength or ductility of magnesium is increased.

2. The addition of nanoparticles to magnesium alloy AZ31B is capable of significantly increasing the: (a) dry oxidation resistance and (b) salt water corrosion resistance of AZ31B. This is significantly more beneficial compared to microparticle addition where typically wet corrosion resistance of magnesium alloy is decreased.

Acknowledgements

Authors wish to acknowledge the National University of Singapore for funding this research through grants and scholarships, and the Agency for Science, Technology and Research (ASTAR) Grant 092 137 0015 (WBS# R-265-000-321-305).

References

- [1] CLYNE, T. W.—WITHERS, P. J.: An Introduction to Metal Matrix Composites. Cambridge, Cambridge University Press 1993.
[doi:10.1017/CBO9780511623080](https://doi.org/10.1017/CBO9780511623080)
- [2] BRANDES, E. A.—BROOK, G. B. (Eds.): Smithells Light Metals Handbook. USA, Reed Educational and Professional Publishing Ltd 1998.
- [3] FERKEL, H.—MORDIKE, B. L.: Mater. Sci. Eng. A, 298, 2001, p. 193. [doi:10.1016/S0921-5093\(00\)01283-1](https://doi.org/10.1016/S0921-5093(00)01283-1)
- [4] HASSAN, S. F.—GUPTA, M.: Comp. Struct., 72, 2006, p. 19. [doi:10.1016/j.compstruct.2004.10.008](https://doi.org/10.1016/j.compstruct.2004.10.008)
- [5] HASSAN, S. F.—GUPTA, M.: J. Mater. Sci., 41, 2006, p. 2229.
- [6] GOH, C. S.—WEI, J.—LEE, L. C.—GUPTA, M.: Nanotechnol., 17, 2006, p. 7.
[doi:10.1088/0957-4484/17/1/002](https://doi.org/10.1088/0957-4484/17/1/002)
- [7] HASSAN, S. F.—GUPTA, M.: J. Alloys Compd., 345, 2002, p. 246. [doi:10.1016/S0925-8388\(02\)00413-9](https://doi.org/10.1016/S0925-8388(02)00413-9)
- [8] PEREZ, P.—GARCES, G.—ADEVA, P.: Compos. Sci. Technol., 64, 2004, p. 145.
- [9] WONG, W. L. E.—GUPTA, M.: Adv. Eng. Mater., 7, 2005, p. 250. [doi:10.1002/adem.200400137](https://doi.org/10.1002/adem.200400137)
- [10] HASSAN, S. F.—GUPTA, M.: J. Alloys Compd., 335, 2002, p. L10.
- [11] HUARD, G.—ANGERS, R.—KRISHNADEV, M. R.—TREMBLAY, R.—DUBE, D.: Canad. Metall. Quart., 38, 1999, p. 193.
[doi:10.1016/S0008-4433\(99\)00006-3](https://doi.org/10.1016/S0008-4433(99)00006-3)
- [12] BAK, S.-H.—LEE, D.-B.: Trans. Nonferrous Met. Soc. China, 19, 2009, p. 871.
[doi:10.1016/S1003-6326\(08\)60367-2](https://doi.org/10.1016/S1003-6326(08)60367-2)
- [13] TIWARI, S.—BALASUBRAMIANIAM, R.—GUPTA, M.: Corr. Sci., 49, 2007, p. 711.
[doi:10.1016/j.corsci.2006.05.047](https://doi.org/10.1016/j.corsci.2006.05.047)
- [14] PARDO, A.—MERINO, S.—MERINO, M. C.—BARROSO, I.—MOHEDANO, M.—ARRABAL, R.—VIEJO, F.: Corr. Sci., 51, 2009, p. 841.
[doi:10.1016/j.corsci.2009.01.024](https://doi.org/10.1016/j.corsci.2009.01.024)
- [15] BAKKAR, A.—NEUBERT, V.: Corr. Sci., 49, 2007, p. 1110. [doi:10.1016/j.corsci.2006.07.002](https://doi.org/10.1016/j.corsci.2006.07.002)

- [16] BAKKAR, A.—NEUBERT, V.: *Electrochimica Acta*, 54, 2009, p. 1597. [doi:10.1016/j.electacta.2008.09.064](https://doi.org/10.1016/j.electacta.2008.09.064)
- [17] NIJNEZ-LOPEZ, C. A.—SKELDON, P.—THOMPSON, G. E.—LYON, P.—KARIMZADEH, H.—WILKST, T. E.: *Corr. Sci.*, 37, 1995, p. 689.
- [18] MEI, Z.—GUO, L. F.—YUE, T. M.: *J. Mater. Proc. Technol.*, 161, 2005, p. 462. [doi:10.1016/j.imatprotec.2004.07.084](https://doi.org/10.1016/j.imatprotec.2004.07.084)
- [19] XUE, W.—JIN, Q.—ZHU, Q.—HUA, M.—MA, Y.: *J. Alloys Compd.*, 482, 2009, p. 208. [doi:10.1016/j.jallcom.2009.03.159](https://doi.org/10.1016/j.jallcom.2009.03.159)
- [20] YUE, T. M.—WANG, A. H.—MAN, H. C.: *Scripta Mater.*, 38, 1998, p. 191. [doi:10.1016/S1359-6462\(97\)00495-8](https://doi.org/10.1016/S1359-6462(97)00495-8)
- [21] GUPTA, M.—LAI, M. O.—LIM, S. C.: *J. Alloys Compd.*, 260, 1997, p. 250. [doi:10.1016/S0925-8388\(97\)00156-4](https://doi.org/10.1016/S0925-8388(97)00156-4)
- [22] NGUYEN, Q. B.—GUPTA, M.: *J. Alloys Compd.*, 459, 2008, p. 244. [doi:10.1016/j.jallcom.2007.05.038](https://doi.org/10.1016/j.jallcom.2007.05.038)
- [23] SZARAZ, Z.—TROJANOVA, Z.—CABBIBO, M.—EVANGELISTA, E.: *Mater. Sci. Eng. A*, 462, 2007, p. 225. [doi:10.1016/j.msea.2006.01.182](https://doi.org/10.1016/j.msea.2006.01.182)
- [24] DAI, L. H.—LING, Z.—BAI, Y. L.: *Comp. Sci. Technol.*, 61, 2001, p. 1057. [doi:10.1016/S0266-3538\(00\)00235-9](https://doi.org/10.1016/S0266-3538(00)00235-9)
- [25] HULL, D.—BACON, D. J.: *Introduction to Dislocations* (4th Ed.). Oxford, Butterworth-Heinemann 2002.
- [26] TROJANOVÁ, Z.—LUKÁČ, P.—SZÁRAZ, Z.: *Kovove Mater.*, 45, 2007, p. 283.
- [27] PAHUTOVÁ, M.—SKLENIČKA, V.—KUCHAROVÁ, K.—SVOBODA, M.—LANGDON, T. G.: *Kovove Mater.*, 43, 2005, p. 34.
- [28] MUKAI, T.—YAMANOI, M.—WATANABE, H.—HIGASHI, K.: *Scripta Mater.*, 45, 2001, p. 89. [doi:10.1016/S1359-6462\(01\)00996-4](https://doi.org/10.1016/S1359-6462(01)00996-4)
- [29] GOH, C. S.—WEI, J.—LEE, L. C.—GUPTA, M.: *Acta Mater.*, 55, 2007, p. 5115. [doi:10.1016/j.actamat.2007.05.032](https://doi.org/10.1016/j.actamat.2007.05.032)
- [30] HASSAN, S. F.—GUPTA, M.: *J. Alloys Compd.*, 429, 2007, p. 176. [doi:10.1016/j.jallcom.2006.04.033](https://doi.org/10.1016/j.jallcom.2006.04.033)
- [31] HASSAN, S. F.—GUPTA, M.: *J. Alloys Compd.*, 419, 2006, p. 84. [doi:10.1016/j.jallcom.2005.10.005](https://doi.org/10.1016/j.jallcom.2005.10.005)
- [32] PARAMSOTHY, M.—HASSAN, S. F.—SRIKANTH, N.—GUPTA, M.: *Mater. Sci. Eng. A*, 527, 2009, p. 162. [doi:10.1016/j.msea.2009.07.054](https://doi.org/10.1016/j.msea.2009.07.054)
- [33] TUN, K. S.—GUPTA, M.: *Comp. Sci. Technol.*, 67, 2007, p. 2657. [doi:10.1016/j.compscitech.2007.03.006](https://doi.org/10.1016/j.compscitech.2007.03.006)
- [34] TUN, K. S.—GUPTA, M.—SRIVATSAN, T. S.: *Mater. Sci. Technol.*, 26, 2010, p. 87. [doi: 10.1179/174328408X388095](https://doi.org/10.1179/174328408X388095)
- [35] PARAMSOTHY, M.—HASSAN, S. F.—SRIKANTH, N.—GUPTA, M.: *J. Nanosci. Nanotechnol.*, 10, 2010, p. 956. PMID:20352742, [doi:10.1166/jnn.2010.1809](https://doi.org/10.1166/jnn.2010.1809)
- [36] PARAMSOTHY, M.—HASSAN, S. F.—NGUYEN, Q. B.—SRIKANTH, N.—GUPTA, M.: *Mater. Sci. Forum*, 618–619, 2009, p. 423. [doi:10.4028/www.scientific.net/MSF.618-619.423](https://doi.org/10.4028/www.scientific.net/MSF.618-619.423)
- [37] DIETER, G. E.: *Mechanical Metallurgy* (SI Metric Edition). London, McGraw-Hill Book Company 1988.
- [38] JAYARAMANAVAR, P.—PARAMSOTHY, M.—BALAJI, A.—GUPTA, M.: *J. Mater. Sci.*, 45, 2010, p. 1170.
- [39] LIM, S. C. V.—GUPTA, M.: *Mater. Sci. Technol.*, 19, 2006, p. 803. [doi:10.1179/026708303225002154](https://doi.org/10.1179/026708303225002154)
- [40] UGANDHAR, S.—GUPTA, M.—SINHA, S. K.: *Comp. Struct.*, 72, 2006, p. 266. [doi:10.1016/j.compstruct.2004.11.010](https://doi.org/10.1016/j.compstruct.2004.11.010)
- [41] BABOIAN, R.: *Corrosion Tests and Standards*, ASTM Manual Series: MNL 20. Fredericksburg, ASTM 1995.
- [42] NGUYEN, Q. B.—GUPTA, M.—SRIVATSAN, T. S.: *Mater. Sci. Eng. A*, 500, 2009, p. 233. [doi:10.1016/j.msea.2008.09.050](https://doi.org/10.1016/j.msea.2008.09.050)
- [43] NGUYEN, Q. B.—GUPTA, M.: *Comp. Sci. Technol.*, 68, 2008, p. 2185. [doi:10.1016/j.compscitech.2008.04.020](https://doi.org/10.1016/j.compscitech.2008.04.020)
- [44] NORDLIEN, J. H.—ONO, S.—MASUKO, N.—NISANCIOGLU, K.: *Corr. Sci.*, 39, 1997, p. 1397. [doi:10.1016/S0010-938X\(97\)00037-1](https://doi.org/10.1016/S0010-938X(97)00037-1)
- [45] SHAMIR, N.—MINTZ, M. H.—BLOCH, J.—ATZMONY, U.: *J. Less Common Met.*, 92, 1983, p. 253. [doi:10.1016/0022-5088\(83\)90492-7](https://doi.org/10.1016/0022-5088(83)90492-7)
- [46] FERRANDO, W. A.: *J. Mater. Eng.*, 11, 1989, p. 299. [doi:10.1007/BF02834140](https://doi.org/10.1007/BF02834140)
- [47] SONG, G.—ATRENS, A.—StJOHN, D.—WU, X.—NAIRN, J.: *Corr. Sci.*, 39, 1997, p. 1981. [doi:10.1016/S0010-938X\(97\)00090-5](https://doi.org/10.1016/S0010-938X(97)00090-5)
- [48] KUKREJA, M.—BALASUBRAMANIAM, R.—NGUYEN, Q. B.—GUPTA, M.: *Corr. Eng. Sci. Technol.*, 44, 2009, p. 381. [doi:10.1179/147842208X356857](https://doi.org/10.1179/147842208X356857)
- [49] GOH, C. S.—WEI, J.—LEE, L. C.—GUPTA, M.: *Mater. Sci. Eng. A*, 423, 2006, p. 153. [doi:10.1016/j.msea.2005.10.071](https://doi.org/10.1016/j.msea.2005.10.071)
- [50] HASSAN, S. F.—GUPTA, M.: *Mater. Sci. Technol.*, 20, 2004, p. 1383. [doi:10.1179/026708304X3980](https://doi.org/10.1179/026708304X3980)